A Novel Asymmetric Interior Permanent Magnet Synchronous Machine

Y. Xiao, Z.Q. Zhu, J.T. Chen, D. Wu, and L.M. Gong

***Abstract* – In this paper, a novel asymmetric interior permanent magnet (AIPM) synchronous machine is proposed. Its asymmetric rotor topology, designated as 1.5-layer permanent magnet (PM) structure, features an asymmetric arrangement of the V-shape PMs and the spoke PMs, together with an asymmetric flux barrier located near the rotor surface in each pole. They are employed to utilize the magnetic-field-shifting (MFS) effect for torque enhancement by reducing the current angle difference between peak PM and reluctance torque components. Effects of geometric parameters of the 1.5-layer rotor design, namely asymmetry and pole arc of V-shape cavity as well as position and dimensions of flux barrier, on maximum torque and air-gap field are investigated. Three machines, i.e. the proposed 1.5-layer AIPM, a 1.5-layer symmetrical rotor topology IPM-I and a conventional single layer V-shape benchmark IPM-II are designed using the same stator, rotor diameters and PM usage by global parametric optimization. Their electromagnetic performance is compared. It confirms that the proposed AIPM has the highest maximum torque. It is also revealed that the torque enhancement is achieved by both 1.5-layer structure and MFS effect.**

***Index Terms*—asymmetric rotor, interior permanent magnet (IPM), magnetic-field-shifting (MFS), reluctance torque, spoke-type PM**

I. INTRODUCTION

INTERIOR permanent magnet (IPM) machines are preferable in commercial applications that require high torque/power, high efficiency, wide constant power speed range (CPSR) and mechanical robustness due to their advantages of superior torque density, outstanding demagnetization withstand capability, and expedient maintenance [1]. Besides, the utilization of reluctance torque in IPMs, originated from the significant difference between *d*- and *q*-axis inductances, can reduce the usage of rare-earth PM material that is unsustainable and expensive, which eases both resource and cost issues [2].

The rotor topologies are crucial for performance improvement of IPM designs. Many IPM rotor structures have been reported in literature and employed in industry [3, 4]. Among them, single layer structures, including spoke-type, V- and flat-shape IPMs, and double layer Delta-shape design are the most popular topologies due to their simple structures and good performance. The three aforementioned single layer topologies, as well as a U-shape structure, are compared in [4] for electric vehicle application, which shows that the highest output torque and power factor are achieved by the V-shape structure and the Spoke-type design has the widest CPSR. The comparison in [5] between the V-shape, U-shape, flat-shape and mixed V- and U-shape topologies indicates that the V-shape structure has the highest maximum average torque, the widest CPSR and the most significant rotor saliency at open-circuit condition.

To increase torque density without more PM usage, multi-layer rotor structures are usually employed to enhance reluctance torque by high saliency. [6] compares IPM topologies with single-, double-, three-, six- and ten-layer circular PMs which shows significant enhancement of maximum torque when the number of PM layer increase from one to two and indicates that the largest rotor saliency is achieved by the triple-layer design. The comparison between V-shape, Delta-shape, double flat-shape and mixed Delta- and U-shape is reported in [7] and [8]. It is found that the highest torque density and highest efficiency are achieved by Delta-shape and mixed Delta- and U-shape designs, respectively. In design of multi-layer IPMs, researchers are also interested in using cheap ferrite PMs to replace rare-earth PMs, thereby significantly reducing the cost of machines and the risk of uncertainty of rare-earth materials, as reported in [9-11]. Except for ferrite PMs, a multi-layer IPM using low cost Al-Ni-Co PMs is also investigated in [12], which shows improvements of torque density, power factor and torque ripple, compared with a synchronous reluctance machine. Nevertheless, complicated structure and many pieces of PMs of multi-layer rotor topologies usually results in difficulty in optimization design and concerns for manufacturing and PM assembly issues.

As symmetrical rotor geometry is generally exhibited in existing IPM designs, an inherent difference of current angles for maximum PM and reluctance torque components exists that is typically 45 electrical degrees (ED), which consequently reduces the utilization ratios of both components in the maximum resultant torque. Accordingly, a novel design concept is proposed by using asymmetric rotor structure to shift the peak points of PM and reluctance torque components to be closer, thereby enhancing the average torque with the same PM usage, which is designated as magnetic-field-shifting (MFS) effect in this paper. In [13] and [14], an IPM design whose rotor exhibits poles using shifted inset PMs and V-shape PMs alternatively is proposed to produce the MFS effect. [15] adds asymmetric flux barrier in a V-shape IPM, which shows a clear increase of average torque. [16] proposes a rotor design with symmetrical cavity design and asymmetric PM configuration that has significant torque enhancement due to MFS effect, but the rotor

Y. Xiao and Z.Q. Zhu are with the Department of Electronic and Electrical Engineering, University of Sheffield, Sheffield, S1 3JD, UK (e-mail: yxiao23@sheffield.ac.uk, z.q.zhu@sheffield.ac.uk)

J. T. Chen, D. Wu and L. M. Gong are with the Midea Shanghai Motors and Drives Research Center, Shanghai, China (e-mail: chenjintao@welling.com.cn, wudi9@welling.com.cn and gongliming@media.com)

structure is complicated.

In this paper, a novel asymmetric IPM (AIPM) topology, designated as the 1.5-layer PM structure, using a pair of V-shape PMs and a spoke-type PM, together with an extra flux barrier near the rotor surface in each pole, is proposed for torque enhancement. The spoke PM structure is regarded as a half layer rather than one layer in the designation because the magnetic motive force (MMF) of a spoke PM and the magnetic reluctance of a spoke PM cavity are shared by magnetic circuits of adjacent poles, both on open-circuit and on-load conditions, which is different from V-shape PMs. The main features of the asymmetric design are angle shifting between axes of V-shape PM cavity and spoke PM cavity, which describes the asymmetry of the V-shape cavity comparing with the adjacent spoke PMs, and the position and dimensions of the extra flux barrier near the rotor surface. Both of these asymmetric features are employed to create MFS effect.

This paper is organized as follows: Section II describes designs of the proposed asymmetric 1.5-layer mixed V-shape and spoke PM AIPM topology, Fig.1(a), the symmetrical 1.5-layer IPM, Fig.1(b), and a conventional V-shape IPM, Fig.1(c), with the same stator, rotor diameters and PM usage. Section III investigates the influences of main geometric parameters of asymmetric feature on maximum torque and open-circuit air-gap field and optimal designs of three topologies are obtained. In Section IV, electromagnetic performances of the proposed AIPM and two symmetrical IPMs are compared to confirm the merits of the proposed topology and to reveal the mechanism of torque enhancement. The conclusion is given in Section V.

II. Proposed Machine Topology

The proposed novel AIPM rotor topology with a 1.5-layer mixed V-shape and spoke PM structure, as well as an extra asymmetric flux barrier near the rotor surface in each pole, is illustrated in Fig. 1 (a). Compared with the symmetrical IPM using 1.5-layer mixed V-shape and spoke PM structure IPM-I as shown in Fig. 1 (b), asymmetry of the V-shape PM cavity can be observed, featured by angle shifting between axes of V-shape PMs and spoke PM cavity and the position and dimensions of the asymmetric flux barrier near the rotor surface that is located between the right side PM of V-shape PMs and its adjacent spoke PM. These features make both cavity design and PM configuration in AIPM exhibit asymmetric distribution and thus MFS effect for torque enhancement. Rectangular PMs with the same dimensions are employed in both AIPM and IPM-I. Besides, a conventional V-shape IPM benchmark IPM-II is designed for comparison as shown in Fig. 1(c), which has the same rotor diameters, iron bridge thickness and total PM volume as AIPM and IPM-I. Magnetization directions of PMs are denoted by arrows in Fig. 1. Besides, the same 24-slot/4-pole integer-slot stator with single-layer distributed windings is applied for all three machine topologies, as shown in Fig. 1(d).

The rotor geometric model of the AIPM is shown in Fig. 2. The *d*-axis of the AIPM is located at the central axis between adjacent spoke PMs, while the *q*-axis remains at the conventional position that has a 90 ED angle difference from the *d*-axis. The position of the V-shape PM cavity is characterized by the angle between central axes of V-shape PMs and spoke PMs, namely θ_{vs}, in each pole, which indicates the asymmetry of V-shape PMs. An asymmetry factor β_{vs} is defined for the asymmetry of V-shape PMs in AIPM, which is defined as

$$\beta_{\mathrm{vs}} = 4p\theta_{vs} / \theta_{cir} \tag{1}$$

where p is the pole pair number and θ_{cir} is the mechanical degree of a whole circle that is 360 degrees.

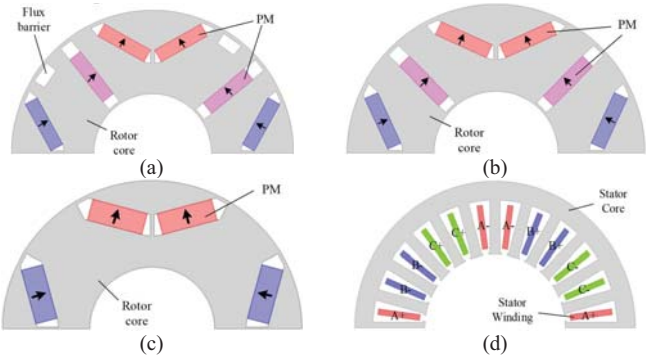

Fig. 1. Machine topologies. (a) Proposed AIPM with asymmetric 1.5-layer mixed V-shape and spoke PMs, as well as extra flux barriers, (b) Symmetrical IPM-I with 1.5-layer mixed V-shape and spoke PM structure, (c) V-shape IPM benchmark IPM-II, (d) Stator design.

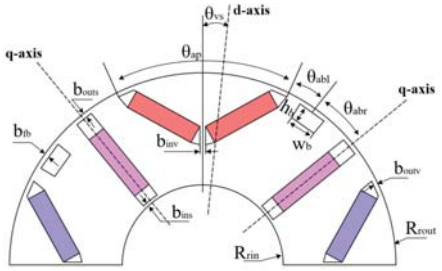

Fig. 2. Rotor geometric model and some key design parameters of the proposed AIPM.

The flux barrier is located near the rotor surface at the right side of V-shape PMs between the V-shape cavity and the adjacent spoke PM, whose position is characterized by arc pitches between the central line of the flux barrier and the right side of PM cavity and the central line of the adjacent spoke PM, respectively, which are designated as θ_{abl} and θ_{abr}, respectively. To simplify the description of the flux barrier position, a position factor β_{pb} is defined as

$$\beta_{pb} = \theta_{abl} / \theta_{abr} \tag{2}$$

The dimensions of the flux barrier are described by the flux barrier width w_b and the thickness h_b. θ_{ap} denotes the pole arc of V-shape PMs in each pole. Outer and inner radii of the rotor are R_{rout} and R_{rin}, respectively, while b_{outv}, b_{inv}, b_{outs}, b_{ins} and b_{fb} are the thicknesses of iron bridges of V-shape cavity, the spoke-type cavity and the flux barrier, respectively.

In general, the symmetrical 1.5-layer mixed V-shape and spoke PM topology IPM-I uses V-shape PMs as the first layer and further employs spoke PMs to create a half layer structure for torque enhancement while reducing the number of PMs, compared with IPM-II. In particular, three PMs with the same dimensions are designed for IPM-I, while the total

PM usage is the same as IPM-II. The proposed AIPM aims to provide further enhancement of average torque by employing asymmetric rotor structure to utilize MFS effect with the same PMs as IPM-I. Besides, only three pieces of PMs are employed in the proposed AIPM and IPM-I, which will not cause considerable increase of costs and difficulty in manufacturing.

III. Effects of Key Rotor Parameters on Machine Performance

In this section, influences of the asymmetry of V-shape cavity, position and dimensions of the extra flux barrier, and pole arc of the V-shape cavity on maximum torque and open-circuit air-gap field are investigated. The time-stepping finite element (FE) analysis is used for electromagnetic performance computation and maximum torque per ampere (MTPA) method is employed for maximum torque calculation. Besides, optimal designs of three topologies are obtained by using genetic optimization algorithm.

A. Effects of V-shape Cavity Asymmetry

Influences of the asymmetry of V-shape cavity, represented by the asymmetry factor β_{vs}, on maximum torque at 10 A current amplitude and on open-circuit air-gap field are shown in Fig .3. The asymmetry factor shows significant influences on maximum torque of AIPM and the optimal design exists. Besides, the increase of asymmetry factor can gradually shift the axis of open-circuit air-gap field, without affecting the shape and magnitude of waveforms.

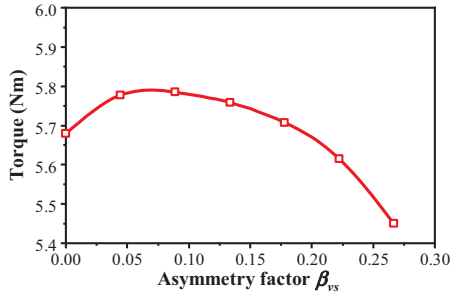

(a)

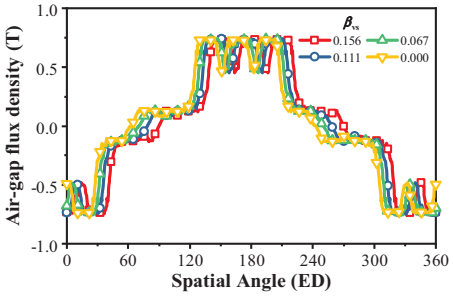

(b)

Fig. 3 Influences of asymmetry factor at 1500 r/min when θ_{ap} = 90 elec.degs (ED), β_{pb} = 0.1, w_b = 2.75 mm and h_b = 2 mm. (a) Maximum torque at 10A current amplitude, (b) Open-circuit flux density waveforms with different asymmetry ratio.

B. Effects of Flux Barrier Position and Dimensions

The effects of the position factor of flux barrier, β_{pb}, are shown in Fig. 4. The position of flux barrier can clearly affect the maximum torque, but has no effect on open-circuit field. The trend of maximum torque via the position factor has two peak points, corresponding to designs when the flux barrier is geometrically near the V-shape cavity and the spoke cavity, respectively, while the optimal value exists when β_{pb} is small, i.e. flux barrier is close to the V-shape cavity.

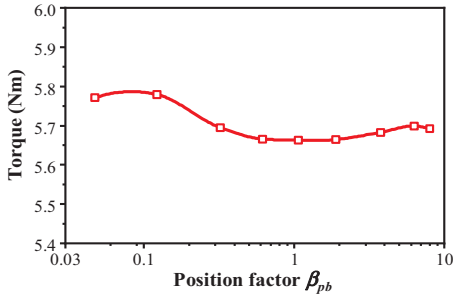

(a)

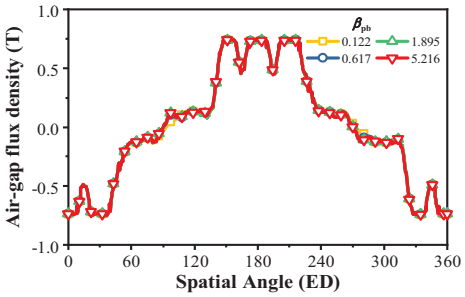

(b)

Fig. 4 Influence of flux barrier position at 1500 r/min when θ_{ap} = 90 ED, β_{vs} = 0.067, w_b = 2.75 mm and h_b = 2 mm. (a) Maximum torque at 10A current amplitude, (b) Open-circuit flux density waveforms with different flux barrier position ratio.

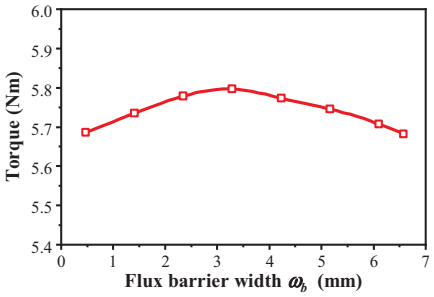

(a)

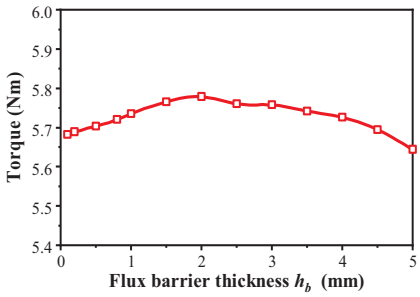

(b)

Fig. 5 Influences of flux barrier dimensions on maximum torque at 1500 r/min and 10A current amplitude when θ_{ap} = 90 ED, β_{vs} = 0.067 and β_{pb} = 0.088. (a) Variation of flux barrier width when h_b = 2 mm, (b) Variation of flux barrier thickness when w_b = 2.75 mm.

The influences of the dimensions of the flux barrier, i.e. the width and thickness, on maximum torque are shown in Fig .5. Optimal values exist for both the width and thickness of the flux barrier. Besides, both flux barrier dimensions have negligible effects on open-circuit field.

C. *Effects of Pole Arc θ_{ap} of V-shape PMs*

The influences of pole arc θ_{ap} of three topologies on maximum torque are compared in Fig. 6. In each design with different pole arc, geometric parameters including the asymmetry of V-shape cavity and position and dimensions of the flux barrier are optimized for maximum torque. As can be seen, the proposed AIPM has the highest maximum torque across the range of pole arc of V-shape cavity, followed by IPM-I with 1.5-layer structure and the conventional benchmark IPM-II has the smallest torque. Besides, optimal pole arc designs of three topologies are achieved at different values and maximum torques of topologies become similar when θ_{ap} is large (near 140 ED). Fig. 6 also confirms that the symmetrical 1.5-layer IPM-I topology has significant torque enhancement comparing with IPM-II with the same PM usage, while a clear torque enhancement can be further achieved from IPM-I with the same PMs by using the proposed asymmetric topology AIPM. However, the increase of maximum torque from IPM-I to AIPM is smaller than that from IPM-II to IPM-I.

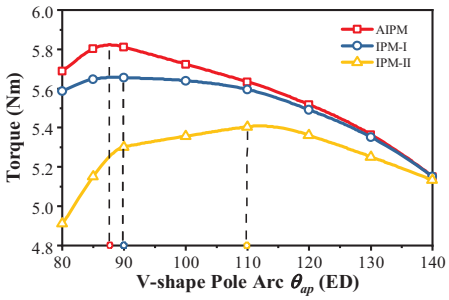

Fig. 6 Variation of maximum torque with different pole arc of V-shape PMs at 10A current amplitude and 1500 r/min, when asymmetric factor and flux barrier parameters of AIPM are optimized in each case.

D. *Global Parametric Optimization*

As a lot of geometric parameters exist in AIPM rotor structure, the global parametric optimization with FE analysis and genetic algorithm is employed to obtain the optimal design. During the optimization process, some design parameters are fixed, including outer and inner radii of rotor, axial lamination length, lamination factor, thicknesses of iron bridges, PM dimensions and stator design. Besides, constant 10 A current amplitude and 1500 r/min rotation speed are employed in operation control while the current advancing angle is optimized by MTPA. The optimization process, whose main target is to maximize the maximum average torque, is also employed for two symmetrical IPM designs. Some key design parameters of final optimal designs of three topologies are listed in Table I and the optimal structures and their open-circuit field and flux line distributions are illustrated in Fig. 7. It shows that the optimal solution of AIPM has the flux barrier connected with the right side of the V-shape cavity, while the V-shape cavity is shifted to be closer to its adjacent spoke PM in the left sides. Both features are consistent with the parametric study results.

TABLE I
MAIN DESIGN PARAMETERS OF THREE TOPOLOGIES

Parameters	Unit	AIPM	IPM-I	IPM-II
No of stator slots, N_s	-		24	
Pole pair number, p	-		2	
The number of turns per phase	-		480	
Air-gap length, δ	mm		1	
R_{rin}	mm		10	
R_{rout}	mm		26.9	
Total PM volume, V_{mag}	mm^3		12600	
PM material and grade	-		Nd-Fe-B, N38	
Remanence, B_r	T		1.235	
Rotor axial length, L_t	mm		50	
θ_{ap}	elec.degs. (ED)	87	90	110
β_{vs}	-	0.067	-	-
β_{pb}	-	0.088	-	
w_b	mm	3.2	-	-
h_b	mm	2.0	-	-
b_{fb}	mm	0.6	-	-

To carry out more detailed investigation and to reveal the mechanism of torque enhancement for the proposed AIPM and IPM-I, electromagnetic performances of three topologies are compared in Section IV.

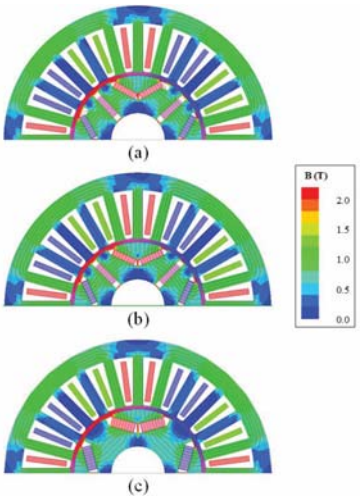

Fig. 7 Open-circuit field and flux line distributions of final optimal designs. (a) AIPM, (b) IPM-I, (c) IPM-II.

IV. COMPARISON OF ELECTROMAGNETIC PERFORMANCE

A. *Open-circuit Characteristics*

Fig. 8 compares the open-circuit air-gap flux density waveforms, spectra and fundamental components of three topologies, respectively. All topologies have similar amplitudes of flux density waveforms and their fundamental components, while the flux density waveform of AIPM exhibits notable distortion and relatively higher total harmonic distortion (THD) and its fundamental component waveform shows a slight but clear axis-shifting effect that indicates the MFS effect, compared with other two symmetrical topologies. The waveforms and spectra of open-circuit back electromotive force (EMF) of Phase A windings in three designs are compared in Fig. 9. The proposed AIPM has the highest amplitude of back EMF, followed by IPM-I, while IPM-II has the smallest, although their differences are

small. Besides, the THDs of back EMF without the 3rd harmonics that are negligible in Y-connection windings in both 1.5-layer topologies are slightly lower than the V-shape benchmark.

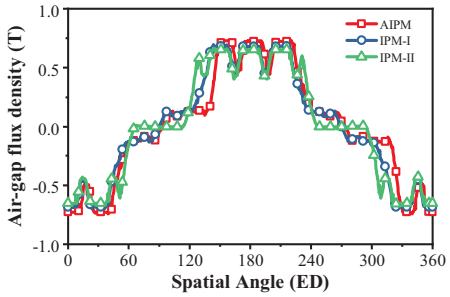

(a)

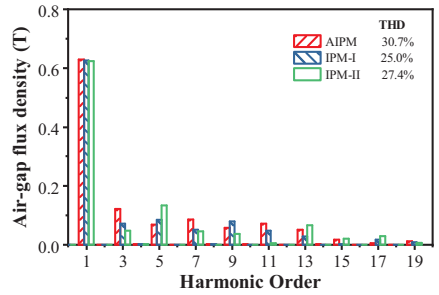

(b)

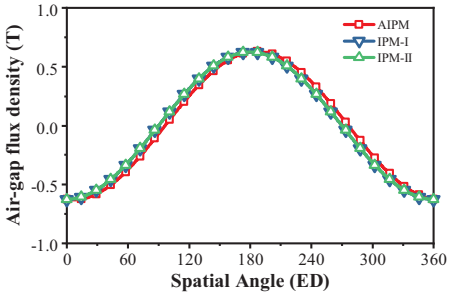

(c)

Fig. 8 Comparison of open-circuit air-gap flux densities. (a) Waveforms, (b) Spectra, (c) Waveforms of fundamental components.

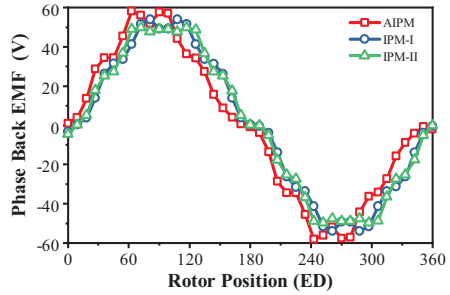

(a)

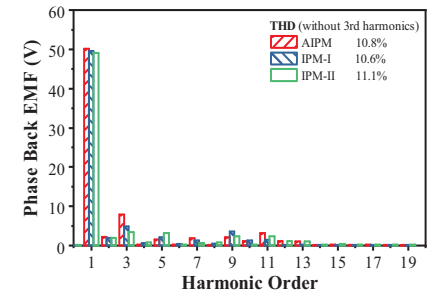

(b)

Fig. 9 Comparison of open-circuit Phase A back EMFs at 1500 r/min. (a) Waveforms, (b) Spectra.

B. On-load Torque Performance

The average torques vs the current advancing angles at 10A current amplitude and 1500 r/min speed of three topologies are compared in Fig. 10. The highest maximum torque is achieved by AIPM, followed by l.5-layer structure IPM-I, and IPM-II has the smallest value. It can also be observed that AIPM reaches the peak average torque at a slightly higher current angle, compared with other topologies. Besides, the average torque of AIPM reaches zero when current advancing angle is about 95 ED, while average torques of both symmetrical topologies become zero when the currant advancing angle is 90 ED, which hints the effect of MFS effect on torque performance.

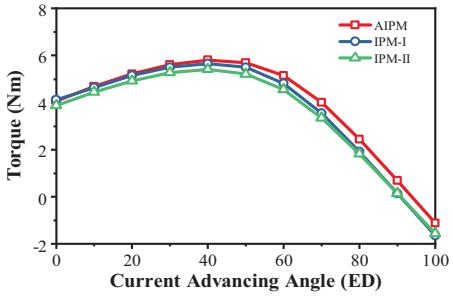

Fig. 10 Average torques vs current advancing angles of three topologies at 1500 r/min and 10A current amplitude.

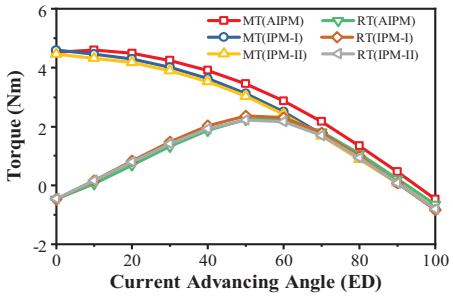

Fig. 11 Torque components via current advancing angles of three topologies at 1500 r/min and 10 A current amplitude.

TABLE II
KEY ON-LOAD PERFORMANCE OF THREE TOPOLOGIES

Performance	Unit	AIPM	IPM-I	IPM-II
T_{syn}^A	Nm	5.80	5.65	5.40
T_m^A	Nm	4.60	4.62	4.45
T_r^A	Nm	2.25	2.40	2.24
Δβ	ED	43	55	58
TE	%	7.40	4.63	-

* T_{syn}^A, T_m^A, T_r^A are amplitudes of average torque, PM torque and reluctance torque, respectively; Δβ is the current angle difference between maximum PM and reluctance torque; TE is the torque enhancement ratio of topologies comparing with IPM benchmark; all at 1500 r/min and 10 A current amplitude.

To find out the mechanism of torque enhancement in both 1.5-layer topologies, torque components of three topologies are extracted using frozen permeability methods [17,18] as shown in Fig. 11, in which MT and RT denote PM and reluctance torque components, respectively. Key performances of torque components are also given in Table II for a clear comparison. The PM torque of AIPM reaches the peak point when current advancing angle is about 10 ED but maximum PM torque points of other two topologies are at 0 ED, while the maximum reluctance torque of three topologies

are achieved at similar current angles. Therefore, there is significant reduction of current angle difference between maximum PM and reluctance torque components in AIPM, compared with two symmetrical designs. In detail, the 1.5-layer symmetrical topology IPM-I has larger maximum PM and reluctance torque and similar △β than the IPM-II. Therefore, it shows a 4.63% increase of maximum torque. The proposed AIPM employs several asymmetric features in the rotor design, compared with the rotor design of IPM-I. Although T_r^A of AIPM is clearly smaller than IPM-I due to asymmetric structure, AIPM has a significantly smaller △β than IPM-I and IPM-II while the amplitudes of PM torque of AIPM and IPM-I are similar because of the similar 1.5-layer PM configuration. Consequently, about 2.65% of torque enhancement in AIPM can be further obtained from IPM-I without introducing any extra costs because the same PMs are employed and only difference is the design of rotor core lamination, while the total torque enhancement ratio of AIPM from IPM-II reaches 7.40%. Thus, it is demonstrated that the torque enhancement of AIPM from the V-shape benchmark IPM-II benefits from both multi-layer structure and MFS effect, and both of these features can provide the increase of maximum average torque effectively when employed individually, as confirmed by the comparison between three topologies. It is also confirmed that the 1.5-layer topology with mixed V-shape and spoke PM structure exhibits similar effects as conventional multi-layer structures especially on the increase of T_r^A and average torque enhancement. In general, the proposed AIPM topology can be a competitive candidate for IPM machine for high torque density applications.

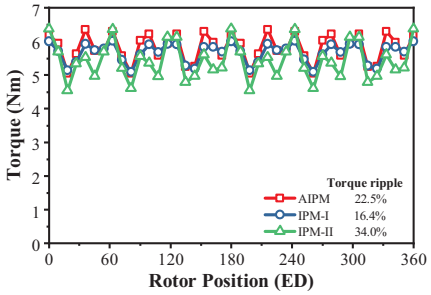

Fig. 12 Torque waveforms at 1500 r/min, 10A current amplitude and current advancing angle for maximum torque.

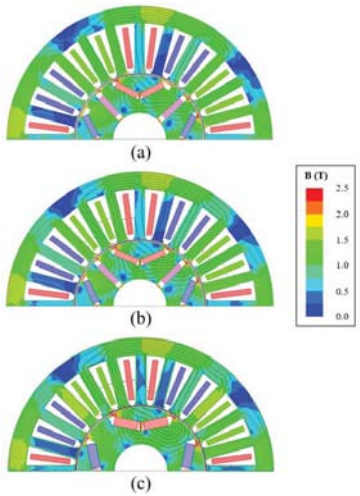

Fig. 13 Comparison of on-load field and flux line distributions of topologies at 1500 r/min, 10A current amplitude and current advancing angle for maximum torque. (a) AIPM, (b) IPM-I, (c) IPM-II.

Fig. 12 compares the torque waveforms and spectra of three topologies at maximum torque conditions. The torque ripple factors are calculated as the ratios between the amplitudes of peak to peak torque fluctuation and the average torque. As can be seen, the torque ripple of AIPM is larger than that of IPM-I, but both values are significantly smaller than the torque ripple of the IPM-II benchmark. The on-load magnetic field and flux line distributions of three topologies at the same conditions for maximum torque in Fig. 12 are compared in Fig. 13.

Fig. 14 compares the maximum torques of three topologies across a wide range of current amplitude, which confirms that no matter at light load, rated load or over load conditions, the AIPM always has the highest maximum torque, followed by IPM-I, while IPM-II is the smallest.

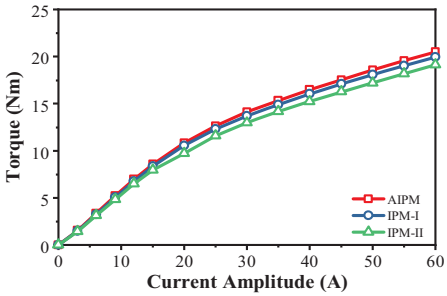

Fig. 14 Comparison of maximum torques vs current amplitudes at 1500 r/min.

C. CPSR Performance

To compare the CPSR performances of topologies, the torque-speed and power-speed curves are obtained [19], as shown in Fig. 15. MTPA control method is employed in the investigation to fully utilize the torque capability.

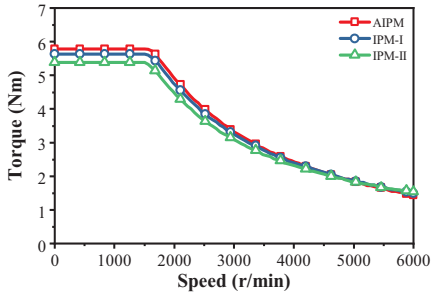

(a)

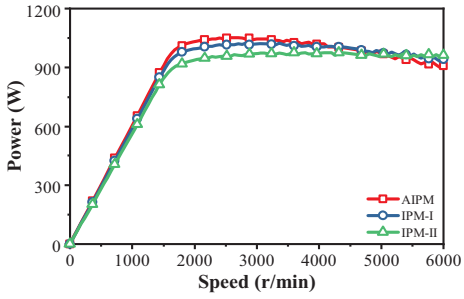

(b)

Fig. 15 Comparison of CPSR performances at DC bus voltage 120V, maximum current amplitude 10A and MTPA control. (a) Torque-speed curve, (b) Power-speed curve.

As shown in Fig. 15, two 1.5-layer topologies, namely AIPM and IPM-I, shows significant torque enhancement in the constant-torque region and the merit remains in the constant-power region at low speed. However, with the increase of speed, the torque/power of both 1.5-layer topologies decrease gradually while the value of IPM-II remains. Specifically, the torque/power of AIPM decreases with a larger gradient, compared with IPM-I. Consequently, the torque/power enhancement of both AIPM and IPM-I diminishes at around 5000 r/min, compared with IPM-II. In general, the proposed 1.5-layer topologies show good CPSR performances for wide speed range, but the significant torque enhancement in the constant-torque region gradually diminishes in the constant-power region with the increase of operation speed.

V. Conclusion

In this paper, a novel AIPM topology featured by the asymmetric 1.5-layer mixed V-shape and spoke PM structure and asymmetric flux barrier in each pole is proposed for torque enhancement. As spoke PMs are employed, the proposed AIPM uses only three pieces of PMs in each pole and has significant torque enhancement comparing with the single-layer V-shape benchmark IPM-II with the same PM usage, while also shows clear increase of average torque comparing with the symmetrical 1.5-layer topology IPM-I with the same dimensions of PMs. The comparison between the proposed AIPM, IPM-I and the benchmark IPM-II using finite element analysis confirms that the torque enhancement is due to both the 1.5-layer PM configuration and MFS effect. The proposed AIPM also shows good CPSR performance although the increase of torque/power gradually diminishes in the constant-power region. A prototype of AIPM is being made and the test results will be reported in due course.

VI. References

[1] Z. Zhu, W. Chu, and Y. Guan, "Quantitative comparison of electromagnetic performance of electrical machines for HEVs/EVs," CES *Trans. on Electr. Mach. and Syst.*, vol. 1, no. 1, pp. 37-47, Jul. 2017.

[2] Z. Zhu and D. Howe, "Electrical machines and drives for electric, hybrid, and fuel cell vehicles," *Proc. IEEE*, vol. 95, no. 4, pp. 746-765, Apr. 2007.

[3] K. Chau, C. C. Chan, and C. Liu, "Overview of permanent-magnet brushless drives for electric and hybrid electric vehicles," *IEEE Trans. Ind. Electron.*, vol. 55, no. 6, pp. 2246-2257, May 2008.

[4] X. Liu, H. Chen, J. Zhao, and A. Belahcen, "Research on the performances and parameters of interior PMSM used for electric vehicles," *IEEE Trans. Ind. Electron.*, vol. 63, no. 6, pp. 3533-3545, Jun. 2016.

[5] K. Kamiev, J. Montonen, M. P. Ragavendra, J. Pyrhönen, J. A. Tapia, and M. Niemelä, "Design principles of permanent magnet synchronous machines for parallel hybrid or traction applications," *IEEE Trans. Ind. Electron.*, vol. 60, no. 11, pp. 4881-4890, Nov. 2013.

[6] Y. Honda, T. Higaki, S. Morimoto, and Y. Takeda, "Rotor design optimisation of a multi-layer interior permanent-magnet synchronous motor," *IEE Proc. – Electr. Power Appl.*, vol. 145, no. 2, pp. 119-124, Mar. 1998.

[7] Y. Hu, S. Zhu, C. Liu, and K. Wang, "Electromagnetic performance analysis of interior PM machines for electric vehicle applications," *IEEE Trans. Energy Convers.*, vol. 33, no. 1, pp. 199-208, Mar. 2018.

[8] S. Zhu, W. Chen, M. Xie, C. Liu, and K. Wang, "Electromagnetic performance comparison of multi-layered interior permanent magnet machines for EV traction applications," *IEEE Trans. Magn.*, vol. 54, no. 11, pp. 1-5, Nov. 2018.

[9] S. Ooi, S. Morimoto, M. Sanada, and Y. Inoue, "Performance evaluation of a high-power-density PMASynRM with ferrite magnets," *IEEE Trans Ind. Appl.*, vol. 49, no. 3, pp. 1308-1315, May-Jun., 2013.

[10] M. Obata, S. Morimoto, M. Sanada, and Y. Inoue, "Performance of PMASynRM with ferrite magnets for EV/HEV applications considering productivity," *IEEE Trans. Ind. Appl.*, vol. 50, no. 4, pp. 2427-2435, Jul.-Aug. 2014.

[11] H. Cai, B. Guan, and L. Xu, "Low-cost ferrite PM-assisted synchronous reluctance machine for electric vehicles," *IEEE Trans. Ind. Electron.*, vol. 61, no. 10, pp. 5741-5748, Oct. 2014.

[12] S. S. Maroufian and P. Pillay, "Design and analysis of a novel PM-assisted synchronous reluctance machine topology with AlNiCo magnets," *IEEE Trans. on Ind. Appl.*, vol. 55, no. 5, pp. 4733-4742, Sep.-Oct. 2019.

[13] X. Zeng, L. Quan, X. Zhu, L. Xu, and F. Liu, "Investigation of an asymmetrical rotor hybrid permanent magnet motor for approaching maximum output torque," *IEEE Trans. Appl. Supercond.*, vol. 29, no. 2, pp. 1-4, Jan. 2019.

[14] G. Liu, G. Xu, W. Zhao, X. Du, and Q. Chen, "Improvement of torque capability of permanent-magnet motor by using hybrid rotor configuration," *IEEE Trans. Energy Convers.*, vol. 32, no. 3, pp. 953-962, Feb. 2017.

[15] W. Zhao, F. Zhao, T. A. Lipo, and B. I. Kwon, "Optimal design of a novel V-type interior permanent magnet motor with assisted barriers for the improvement of torque characteristics," *IEEE Trans. Magn.*, vol. 50, no. 11, pp. 1-4, Dec. 2014.

[16] F. Xing, W. Zhao, and B. I. Kwon, "Design and optimisation of a novel asymmetric rotor structure for a PM-assisted synchronous reluctance machine," *IET Electr. Power Appl.*, vol. 13, no. 5, pp. 573-580, May 2018.

[17] Z.Q. Zhu and W.Q. Chu, "Advanced frozen permeability technique and applications in developing high performance electrical machines," *Trans. of China Electrotech. Soc.*, vol.31, no.20, pp.13-29, Oct. 2016.

[18] G. Qi, J. T. Chen, Z. Q. Zhu, D. Howe, L. B. Zhou and C. L. Gu, "Influence of skew and cross-coupling on flux-weakening Performance of permanent-magnet brushless AC machines," *IEEE Trans. Magn.*, vol. 45, no. 5, pp. 2110-2117, 2009.

[19] W. Q. Chu, Z. Q. Zhu, J. Zhang, X. Liu, D. A. Stone, and M. P. Foster, "Investigation on Operational Envelops and Efficiency Maps of Electrically Excited Machines for Electrical Vehicle Applications," *IEEE Trans. Magn.*, vol. 51, no. 4, pp. 1-10, Apr. 2015.

VII. Biographies

Y. Xiao received the B.Eng. and Ph.D. degrees in electrical engineering from Huazhong university of Science and Technology, Wuhan, China, in 2013 and 2018, respectively. Since 2018, he has been working towards his second Ph.D. degree at the University of Sheffield, U.K. His current research interests include the design of permanent magnet machines.

Z.Q. Zhu has been with the University of Sheffield since 1988, where he currently holds the Royal Academy of Engineering/Siemens Research Chair and is the Head of the Electrical Machines and Drives Research Group. His current major research interests include the design and control of permanent magnet machines and drives for applications ranging from automotive through domestic appliances to renewable energy.

J.T. Chen received the Ph.D. degree in electrical engineering from the University of Sheffield, Sheffield, U.K., in 2009. He is currently a General Manager of Midea Automotive Components Ltd and also with the Midea Shanghai Motors and Drives Research Center, Shanghai, China. His major research interests include the design of permanent magnet machines.

D. Wu received the Ph.D. degree in electronic and electrical engineering from the University of Sheffield, Sheffield, U.K., in 2015. He is currently working with the Midea Shanghai Motors and Drives Research Center, Shanghai, China, as a Research and Development Engineer. His major research interests include the design of permanent magnet machines.

L.M. Gong received the Ph.D. degree from The University of Sheffield, Sheffield, U.K., in 2012. He is currently in charge of the Midea Shanghai Motors and Drives Research Center, Shanghai, China. His research interests include control of permanent magnet machine drives and power electronics.